Research article

Wei-Nan Liu, Rui Chen, Wei-Yi Shi, Ke-Bo Zeng, Fu-Li Zhao and Jian-Wen Dong*

Narrow-frequency sharp-angular filters using all-dielectric cascaded meta-gratings

https://doi.org/10.1515/nanoph-2020-0141
Received February 24, 2020; accepted April 30, 2020;
published online June 17, 2020

Abstract: Selective transmission or filtering always responds to either frequency or incident angle, so as hardly to maximize signal-to-noise ratio in communication, detection and sensing. Here, we propose compact meta-filters of narrow-frequency sharp-angular transmission peak along with broad omnidirectional reflection sidebands, in all-dielectric cascaded subwavelength meta-gratings. The inherent collective resonance of waveguide-array modes and thin film approximation of meta-grating are employed as the design strategy. A unity transmission peak, locating at the incident angle of 44.4° and the center wavelength of 1550 nm, is demonstrated in a silicon meta-filter consisting of two-layer silicon rectangular meta-grating. These findings provide possibilities in cascaded meta-gratings spectroscopic design and alternative utilities for high signal-to-noise ratio applications in focus-free spatial filtering and anti-noise systems in telecommunications.

Keywords: cascaded meta-gratings; Fabry-Perot; spectral and angular selectivity; subwavelength grating.

1 Introduction

Spectral filtering technology has always been the focus of photonics research. Conventional low-loss spectral filters are implemented by dielectric materials and always consist of a defective spacing layer and two pairs of highly reflective thin films including 10–100 layers of quarter-wave plates [1]. Such a large number of layers is required because more layers of alternate high and low index thin films could provide greater optical admittance, which would induce a higher reflection band. This filtering scheme challenges the process and cost-management of fabrication due to the remarkable thin-film inhomogeneity of thickness and density. Besides, internal stress between high and low refractive index quarter-wave layers also hinders the utility of thin-film devices in high power laser system [2]. Angular filters or spatial filters also received much attention since they are widely used in focus-free system [3, 4], solar cell [5, 6] and free space optical telecommunication [7, 8]. Candidates of angular selectivity schemes include multi-layer thin-film [9–11], photonic crystals [12–14], volume bragg gratings [15–17] and rugate thin-film [18–20]. It is noted that the spectral and angular filtering at the same time was first manifested by combining one-dimensional defective photonic crystals [21, 22]. The defective-mode based technology permits transmission center wavelength and angle with narrow passband ($0.0005\lambda_0$, where λ_0 is the center wavelength) and sharp breadth of incident angle (±3°). However, since each of the defective photonic crystals consists of 10th of thin-film layers with precisely controlled thicknesses, the fabrication is challenging.

Recently, subwavelength meta-grating (MG) which takes advantage of its planar structure can be conveniently patterned by various methods, and is widely used in versatile spectral design [23–33]. The coupling of incident light to the guided modes in grating waveguide [34] or the coupling between propagating waveguide array modes (WAMs) inside the grating [35] explains the spectral responses such as broadband high reflectance [36–41], band-pass [42] and band-stop [43]. Another property of MG is that it is capable of providing concurrent angular and spectral selectivity, but in a reflective manner, which needs an additional beam splitter for focus-free application [44]. High-efficiency transmission angular and spectral selectivity is expected.

In this paper, we propose a compact transmission meta-filter scheme of narrow-frequency sharp-angular selectivity (spectral and angular filtering at the same time) that covers wide range omnidirectional reflection band. A narrow-frequency sharp-angular filter is formed by two cascaded silicon rectangular sub-gratings, due to the

Wei-Nan Liu and Rui Chen: These authors contributed equally.

***Corresponding author: Jian-Wen Dong**, School of Physics & State Key Laboratory of Optoelectronic Materials and Technologies, Sun Yat-sen University, Guangzhou, 510275, China, E-mail: dongjwen@mail.sysu.edu.cn

Wei-Nan Liu, Rui Chen, Wei-Yi Shi, Ke-Bo Zeng and Fu-Li Zhao: School of Physics & State Key Laboratory of Optoelectronic Materials and Technologies, Sun Yat-sen University, Guangzhou, 510275, China

Open Access. © 2020 Wei-Nan Liu et al., published by De Gruyter. This work is licensed under the Creative Commons Attribution 4.0 International License.

inherent collective resonance of WAMs in the two sub-gratings and the Fabry–Perot (FP) interference in between. The two sub-gratings of the meta-filter have complementary reflectivity spectra and operate in non-diffractive region. The sub-gratings are spaced far enough to avoid near-field coupling. In addition, we discuss the design flexibilities and versatilities of the filters. The cascaded meta-gratings scheme could provide tunable bandwidth of transmission peak and symmetrical spectrum, which may provide potentials for applications in focus-free system, sensing and telecommunications.

2 WAM analysis of highly reflective meta-grating

The scheme of a narrow-frequency sharp-angular filter consists of two cascaded MGs, as shown in Figure 1A. Two MGs are spaced by certain distances t_s and all their grating bars are invariant along y direction. The top and bottom sub-gratings are suspended in air or immersed in atmospheric materials. The MG-air structure has larger refractive index contrast that may provide higher and broader reflection background [45], while the immersed structure is more fabrication-friendly and shows potential in large-area production [46, 47]. In Figure 1B, the transmission surface diagram shows a narrow-frequency and sharp-angular peak. This device selectively transmits light with certain incident angle θ_O (44.4°) and wavelength λ_O (1550 nm) and reflects all the light with other incident angles ($\theta \neq \theta_O$) or wavelengths ($\lambda \neq \lambda_O$) under TM-polarized light (electric field perpendicular to the grating bars). To explain the spectral response, the broadband high reflectance of single-layer sub-gratings should be carefully investigated since an FP configuration with two highly reflective mirrors is used to generate transmission peak. As shown in Figure 1A, a single-layer MG is characterized by the following parameters: the period Λ, the width of bar s and gap a, thickness t_g and the refractive index of grating n_g and atmospheric material n_a. The ratio of s to Λ is the duty cycle d_c. We analyze a TM polarized plane wave of wavelength λ propagating in the x–z plane using WAM expansion as shown in Figure 2A. The wave number of incident light is k_O and the wave number along x direction is k_x; n is the number of diffraction orders. By matching Bloch boundary conditions at the interfaces between bars and gaps, one can solve the eigenvalue equation of transverse mode profile to derive propagation constant (β) and transverse wave numbers (k_s and k_a) [31, 48],

$$\beta^2 = (2\pi n_a/\lambda)^2 - k_a^2 = (2\pi n_g/\lambda)^2 - k_s^2, \tag{1}$$

$$\begin{aligned} &k_a k_s (n_g/n_a)^2 \left[1 + e^{2ik_x\Lambda} - 2\cos(k_s s)\cos(k_a a)e^{ik_x\Lambda}\right] \\ &+\sin(k_s s)\sin(k_a a)\left[k_a^2 (n_g/n_a)^4 + k_s^2\right]e^{ik_x\Lambda} = 0, \end{aligned} \tag{2}$$

Figure 2B shows the θ-β relation at $\lambda = 1550$ nm of the excited modes in the silicon ($n_g = 3.48$) grating standing in air ($n_a = 1.0$). It is noted that only TM_0 and TM_1 modes are excited from 0 to 90 degree, since the higher order modes (TM_2, TM_3, etc.) are cut-off at this wavelength. Generally, there are m excited WAMs inside the grating layer and n diffraction orders outside. The WAMs are coupled with each other and contribute to the reflection of every diffraction order. Mathematically, the equation correlates the transmission coefficient of a certain diffraction order (τ_n) with the mth modal contribution (χ_{nm}) is [35]:

$$\tau_n = \sum_m \chi_{nm}, \tag{3}$$

According to grating equation, only zeroth diffraction order will propagate in the case of a subwavelength-scale period. For gratings standing in the air, the criterion is:

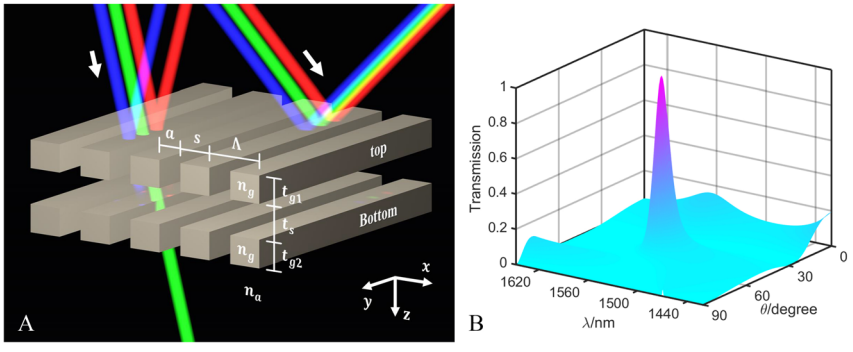


Figure 1: Schematic illustration of narrow-frequency sharp-angular filter using cascaded meta-gratings (MGs).
(A) Scheme of a narrow-frequency sharp-angular filter, consisting of two parallel rectangular dielectric MGs. The grating bars with high refractive index n_g are surrounded by atmospheric medium with low refractive index n_a. (B) The transverse-magnetic (TM) transmission surface diagram of the narrow-frequency sharp-angular filter shows simultaneously angular and spectral transmission selectivity of incident light.

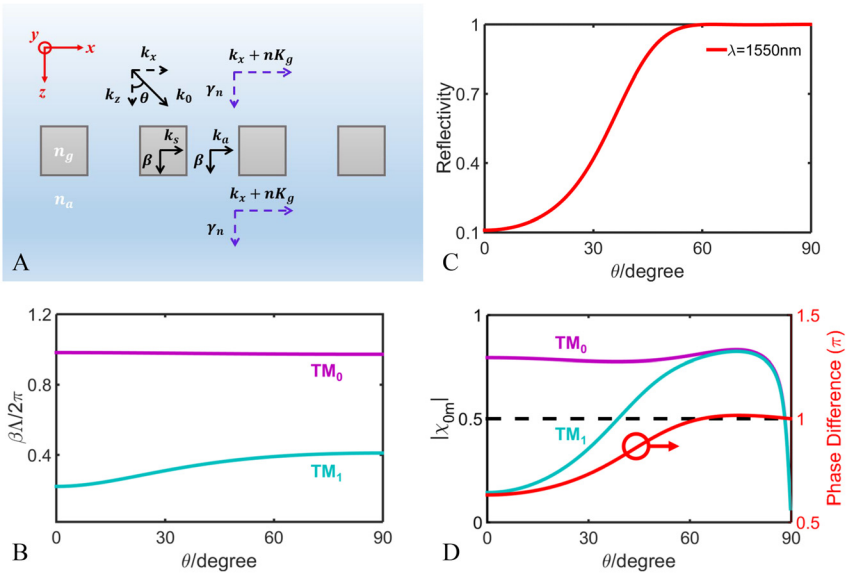


Figure 2: Waveguide array mode expansion and wide-angle high reflectance of single-layer meta-grating (MG) at a given working wavelength.
(A) Cross section of a single-layer MG immersed in surrounding medium and the wave vectors at different regions. (B) Waveguide array mode (WAM) dispersion (θ-β relation) of TM modes at λ = 1550 nm for silicon MG immersed in atmospheric air (d_c = 0.58, Λ = 568 nm). (C) Wide-angle high reflectance of the single-layer MG. (D) Destructive interference of the first two modes in large-angle region.

$$\lambda > (1 + \sin\theta)\Lambda, \tag{4}$$

For the case in Figure 2 ($\lambda \approx 2.73\Lambda$, λ = 1550 nm and Λ = 568 nm) this criterion is satisfied. Therefore, we can achieve a near 100% reflectance if zeroth order transmission is zero, i. e., $\tau_0 = \sum_m \chi_{0m} = 0$. Such example of single-layer MG (t_g = 568 nm, d_c = 0.58) providing near 100% zeroth order reflectivity from 60° to 90° is shown in Figure 2C, which is computed by WAM method [49]. In Figure 2D, the contributions to the 0th order transmission of the two modes (χ_{00} and χ_{01}) are illustrated, which possess nearly the same magnitudes ($|\chi_{00}| = |\chi_{01}|$) but opposite phases across the high-reflectance angles. The completely destructive interference leads to near 100% reflectivity and maintains in wide-angle regime, generating a broad and high reflectance spectrum.

3 Reflectivity of the two sub-gratings forming narrow-frequency sharp-angular filter

A narrow and high transmission peak will arise when two highly reflective mirrors are set in parallel and make up an FP cavity. However, in terms of the two-layer MG configuration, if one of the MGs produces more than one diffraction orders, there will be power redistribution between different orders; on the other hand, in the case that only zeroth order propagates, if the gratings are set too close to each other, the near field coupling of evanescent diffraction orders would come into effect. There will be additional electromagnetic field amplitude and accumulated phase of evanescent order within the penetration depth, which will influence the reflection of the zeroth diffraction. These all hinder the two-layer MG cavity from generating a narrow and near 100% transmission peak.

The sub-gratings of narrow-frequency sharp-angular filter in this paper work in the condition that the distance between sub-gratings is larger than the penetration depth of the first evanescent order ($t_s > 0.3\lambda$ for $\lambda = 2.73\Lambda$) and only zeroth order propagates. The contributions of high order evanescent waves could be ignored and the overall reflectance of a single-layer MG could be effectively considered as a scaler. The single-layer MGs now function as thin films and the cascaded MGs configuration could be analyzed by classical FP model.

The top and bottom sub-gratings have the same period Λ and a duty cycle of d_c = 0.58 is chosen to guarantee that the sub-gratings operate in the dual-mode regime [45] across omnidirection. The sub-gratings use the same material (silicon), but the thicknesses of them are different (t_{g1} = 0.8Λ, t_{g2} = 1.0Λ), leading to different reflectivity spectra. According to the theory of FP cavity consisting of different reflective mirrors whose reflectance coefficients are r_1 and r_2, the total reflection coefficient (r_f) and reflectivity (R_f) are:

$$r_f = \frac{r_1 - r_2 e^{i(2\varphi_1 + 2\delta)}}{1 - r_1 r_2 e^{2i\delta}}, \tag{5}$$

$$R_f = |r_f|^2 = \frac{|r_1|^2 + |r_2|^2 - 2|r_1||r_2|\cos(\Phi)}{1 + |r_1|^2|r_2|^2 - 2|r_1||r_2|\cos(\Phi)}, \tag{6}$$

where $\Phi = \varphi_1 + \varphi_2 + 2\delta$ is the phase factor. φ_1 and φ_2 are the reflection phases of top and bottom sub-gratings. δ is the propagating phase accumulated when light transmits from the top to the bottom of the middle spacing layer. The FP resonance ($R_f = 0$) condition is:

$$\begin{aligned} |r_1| &= |r_2|, \\ \Phi &= 2k\pi, \end{aligned} \tag{7}$$

where k is an integer. The two equations in (7) are the magnitude and phase criteria for high transmission filtering, respectively.

The two sub-gratings' reflectivity contours as a function of wavelength and incident angle are computed by WAM method, as illustrated in Figure 3. Both sub-gratings present broadband wide-angle high reflectance and nearly complementary spectra, i. e., the top sub-grating is of high reflection at angles lower than 44.4° (Figure 3A), while the bottom is of high reflection when the incident angle is larger than 44.4° (Figure 3B). To investigate the high transmission filtering criteria, the two sub-gratings' reflection amplitude differences ($|r_1|-|r_2|$) and the phase factor (Φ) contour as a function of wavelength and incident angle are shown in Figure 3C,D, respectively. Here, the spacing between the two sub-gratings is $t_s = 1.0\Lambda$. The white curves in Figure 3C,D indicate the wavelength and incident angle that satisfy the magnitude ($|r_1| = |r_2|$) and phase criteria ($\Phi = 2k\pi$), respectively. Figure 3E is the reflectivity contour of the narrow-frequency sharp-angular filter and the two white curves in Figure 3C,D are superimposed on it. The two white curves precisely cross at the point where the high transmission (low reflection) peak locates at (λ = 1550 nm, θ = 44.4°). In Figure 3F, the reflection phase contour of the narrow-frequency sharp-angular filter shows that the high transmission point is a phase singularity, where the phase value would alternate by π. These phenomena indicate that the simultaneously angular and spectral filtering is attributed to the FP resonance between the top and bottom sub-gratings.

The reflection contours in Figure 3 also explain the broadband omnidirectional reflection background. Though the FP resonance condition is satisfied at only one wavelength and one angle, if both sub-gratings are of high transmission at another angle or wavelength, according to Eq. (6) the two-layer meta-grating interference would also generate a high transmission response at that angle or wavelength. However, the top and bottom sub-gratings'

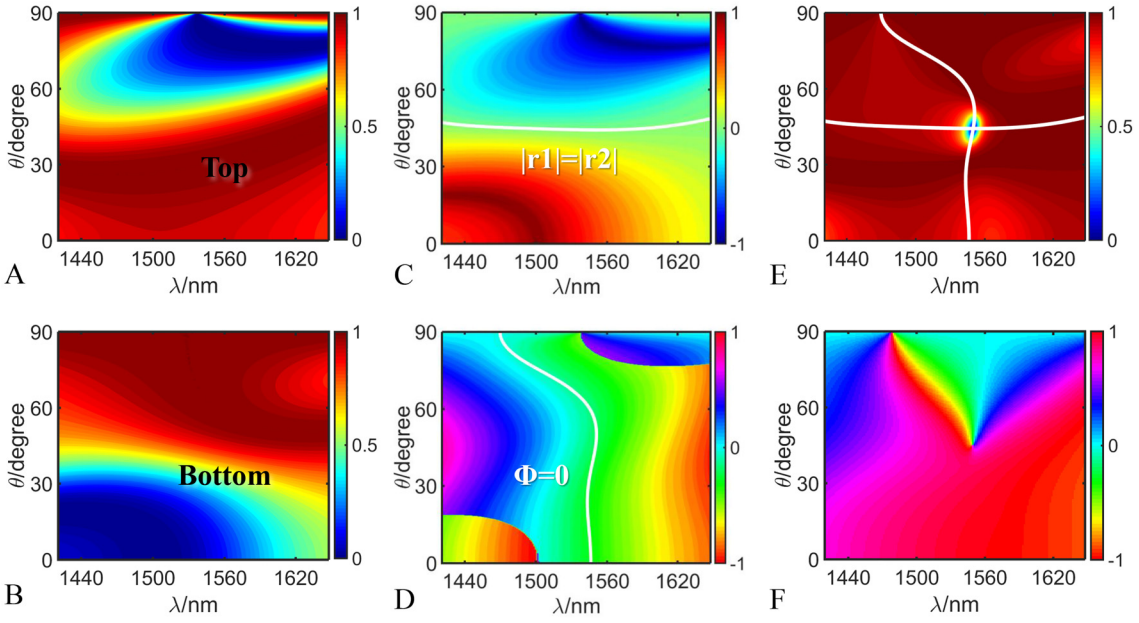


Figure 3: Narrow-frequency sharp-angular filtering explained by two highly reflective meta-grating (MG)s' complementary spectra. (A, B) Reflectivity contours of the top and bottom sub-gratings as a function of wavelength and incident angle. ($t_{g1}b = 0.8\Lambda$, $t_{g2} = 1.0\Lambda$, $\Lambda = 568$ nm). (C) The contour of top and bottom sub-gratings' reflection amplitude differences as a function of wavelength and incident angle. The white curve indicates the wavelength and incident angle that satisfy the magnitude criterion ($|r_1| = |r_2|$). (D) Phase factor (Φ) contour (the unit of color bar is π) as a function of wavelength and incident angle. The white curve indicates the wavelength and incident angle that satisfy the phase criterion ($\Phi = 0$). ($t_s = 1.0\Lambda$). (E) Reflectivity contour of the narrow-frequency sharp-angular filter as a function of wavelength and incident angle. The white curves in (C) and (D) are superimposed on it. (F) Reflection phase contour of the narrow-frequency sharp-angular filter as a function of wavelength and incident angle (the unit of color bar is π).

reflectivity are nearly complementary, at least one of the sub-gratings presents low transmission at every wavelength and angle in the contours of Figure 3. Therefore, except for the point where the incident angle and wavelength satisfy FP resonance condition, other angles and wavelengths should be highly reflective. Note the current design of meta-filter works for TM polarization only since the two sub-gratings will not show complementary broadband wide-angle high reflectance under TE incidence (results not shown here).

To fully investigate the nearly complementary reflectivity of the two sub-gratings, we compute the reflectivity and reflection phase contour as a function of wavelength and grating thickness in Figure 4. The solid white and pink curves in Figure 4(A-D) bounding the reflectivity pattern denote the collective FP resonance of the zeroth and the first WAMs, respectively, which comes from the resonance of the excited assembly of modes [50]. The corresponding mode will experience π phase change across the curves in Figure 4C,D, making a constructive interference transform into a destructive interference and *vice versa*. When the incident angle is 0°, the high reflection region at lower left of Figure 4A is bounded by two resonance curves of the zeroth order mode. Reflectivity spectra of two single-layer MGs with thicknesses 0.8Λ and 1.0Λ (The blue and red dot dash lines in Figure 4A) are plotted in Figure 4E, which indicate the top sub-grating is of high reflection near 1550 nm at low angle.

When the incident angle increases to 80°, the resonance curves of the zeroth and the first modes shift to the longer wavelength direction, making the low reflection region bounded by the resonance curves of the zeroth and the first modes shift to the wavelength period of 1300 ~ 1800 nm, as shown in the lower left of Figure 4B. Under this large angle incidence, the bottom sub-grating is of high reflection near 1550 nm, which is reflected in Figure 4F.

4 Discussions of cascaded meta-grating filters

The FP resonance mechanism provides possibilities of tuning the filtering angle and wavelength since both the phase and magnitude criteria in Equation (7) are subject to the reflection of the two sub-gratings and the phase accumulated in the middle spacing layer. For instance, if the thickness of the middle spacing layer decreases, δ could be reduced. The white curve in Figure 3D shift to the lower wavelength direction and cross with the magnitude curve at a lower wavelength but higher angle, inducing the

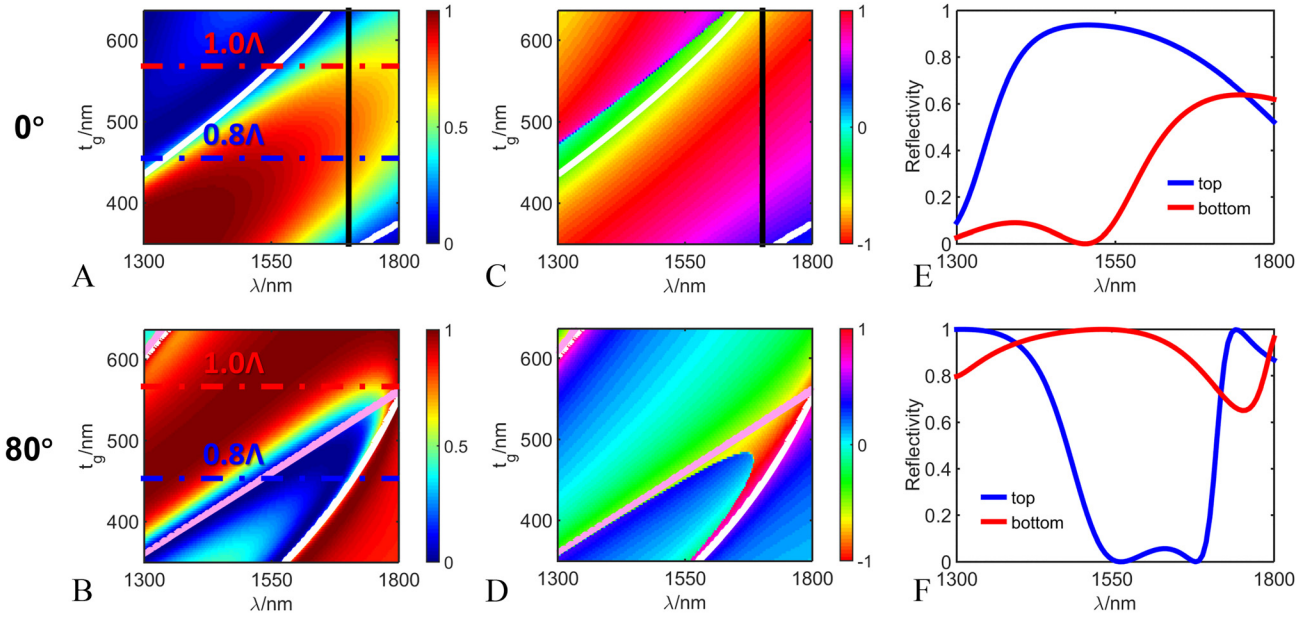


Figure 4: Illustration of the dependence on wavelength and thickness of single-layer meta-grating (MG) at different angles of incidence. (A, B) Reflectivity contour and (C, D) Reflection phase contour (the unit of color bar is π) of single-layer MG as a function of wavelength and grating thickness at the incident angles of 0° and 80°. The black solid line is the cut-off wavelength of the first order waveguide array mode. The white and pink curves are the collective FP resonance curves of the zeroth and the first waveguide array modes, respectively. (E, F) Complementary reflectivity spectra of two single-layer meta-gratings with thicknesses 0.8Λ and 1.0Λ, which are the top and bottom sub-gratings of the narrow-frequency sharp-angular filter in Figure 3, at the incidence angles of 0° and 80°.

transmission center to move to the new FP resonance wavelength and angle. Note that the normal incidence narrow-frequency sharp-angular filter is challenging since the angular reflectivity of top and bottom sub-gratings should cross only at the incident angle of 0°. Besides, one of the sub-gratings should be omnidirectional highly reflective to achieve omnidirectional reflection background (otherwise the spectra of the two sub-gratings cross at another angle and breach the magnitude criterion), which demands much higher permittivity than silicon [51].

Flexibility in tuning the filtering bandwidth is favored since some astronomic and laser applications require extremely narrow bandwidth [17, 52]. As an example, Figure 5A shows the transmission surface diagram of a narrow-frequency sharp-angular filter designed by XGBoost machine-learning method [53]. It is found that this optimized design not only exhibits narrower bandwidth and sharper breadth of incident angle, but also produces broader reflection background than the designed filter in Figure 3. Besides, higher reflective mirrors will induce higher finesse spectrum. One of the strategies to achieve this is by changing the period of one of the sub-gratings. Figure 5B shows the optimized filter's structure with variant top sub-gratings' period. The spectra of the two silicon sub-gratings are demonstrated in Figure 5C. The blue curves correspond to top sub-gratings with three different periods (I, II, III correspond to period 1.0Λ, 0.99Λ, 0.98Λ, respectively) while the red curve is the spectrum of the bottom sub-grating with the same period as top sub-grating I. Filters formed by the top sub-grating I, II, III and the bottom one generate the transmission peak I, II, III at oblique incidence (θ = 44.3°), as shown in Figure 5D. The mechanism underlying the spectrum shift in Figure 5C,D is scaling law, which provides possibilities of tuning the center wavelength and spectrum bandwidth.

Compared with single-layer MG, the cascaded MGs scheme also presents some advantages in optimizing spectrum shape. We plot the linear zero-order transmission (T_0) of a single-layer resonant waveguide meta-grating (RWMG) bandpass filter [42] and a two-layer narrow-frequency sharp-angular filter in linear (Figure 5E) and log scale (Figure 5F). The two-layer structure demonstrates much lower sideband and a more symmetric high-transmission peak while it supports filtering of both angle and

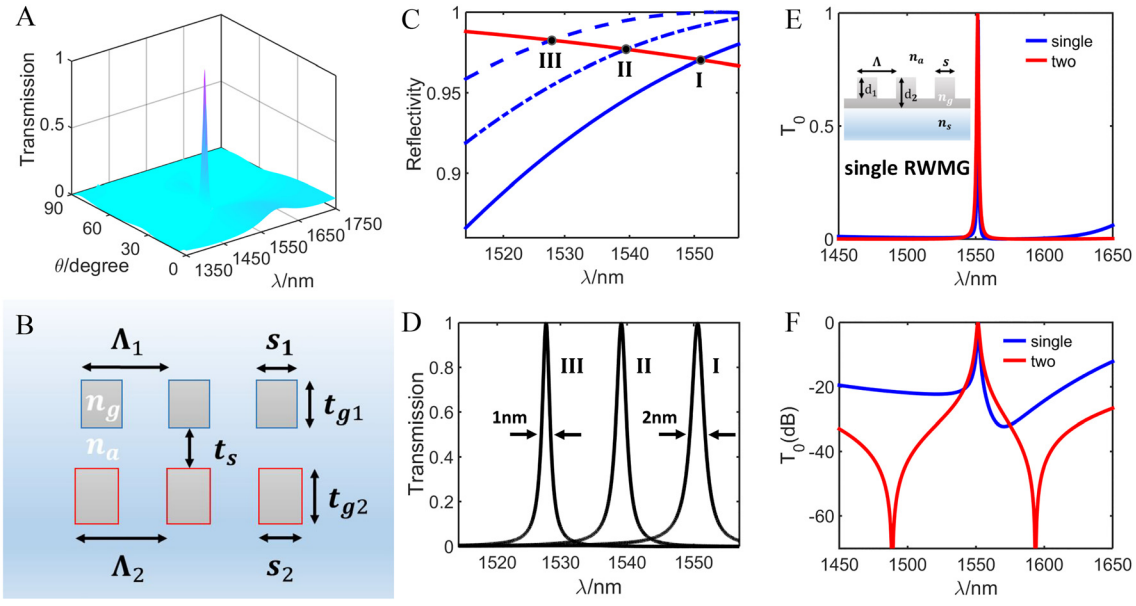


Figure 5: Bandwidth adjustment and symmetricity improvement.
(A) Transmission surface diagram of optimized narrow-frequency sharp-angular filter. (Λ = 537 nm, t_{g1} = 0.69Λ, t_{g2} = 1.01Λ, t_s = 0.86Λ d_c = 0.74, n_g = 3.48, n_a = 1.0, TM mode). (B) Structure of the optimized narrow-frequency sharp-angular filter with different top sub-gratings' period. (C) Reflectivity spectrum of top (blue curves I, II, III are the spectra for gratings of period Λ_1 = 1.0Λ, 0.99Λ, 0.98Λ, respectively) and bottom (red curve) sub-gratings (grating period Λ_2 = 1.0Λ). (D) Three transmission peak spectra of the narrow-frequency sharp-angular filters consisting of top sub-gratings I, II, III respectively and the bottom sub-grating. To satisfy FP resonance condition, the thicknesses of middle spacing layers (t_s) for spectra I, II, III are 0.86Λ, 0.80Λ, 0.75Λ, respectively. (E) Linear zero-order transmission (T_0) of a single-layer RWMG (inset: Λ = 1022 nm, d_1 = 327 nm, d_2 = 618 nm, s/Λ = 0.24, n_g = 3.48, n_s = 1.51, n_a = 1.0, normal incidence, TE mode, computed by finite element method) and a two-layer silicon MG filter (Λ = 537 nm, t_{g1} = 370 nm, t_{g2} = 542 nm, t_s = 461 nm, s/Λ = 0.74, n_g = 3.48, n_a = 1.0, θ = 44.1°, TM mode) centered at 1552 nm and 1551 nm in air, respectively. (F) Log-scale transmission of the single-layer RWMG and two-layer MG.

wavelength. The better symmetricity comes from the coupling of two kinds of resonances: the WAM resonance in the single-layer sub-grating and the FP resonances owing to the cavity. The spectral symmetricity is also tunable by shifting the sub-grating's position along the periodic direction, depending on the shift's perturbation to the FP resonance condition [54].

5 Conclusion

In conclusion, a compact polarization-sensitive meta-filter of narrow-frequency sharp-angular transmission is presented by using cascaded dielectric meta-gratings. The simultaneous implementation of narrow-frequency and sharp-angular can be attributed by the analysis of WAM and FP resonance. The proposed meta-filters possess few-layer structure with thickness confined to the wavelength magnitude, making it more compact and easier integration than the bulky thin film devices. Several methods are applicable to fabricate and characterize few-layer devices [41–43]. Further, such meta-filter not only provides adjustable wavelength and angle selective responses covering wide range of omnidirectional reflection band, but also shows potentials in tunable bandwidth and spectrum symmetricity. In a word, extraordinary narrow-frequency sharp-angular filter may provide improved signal-to-noise ratio and more filtering degrees of freedom. We envision this work could pave the way for spectroscopic study of multilayer meta-grating, for the applications of spectral and angular filtering such as focus-free spatial filter and telecommunication anti-noise systems.

Acknowledgements:: This work is supported by the State Key Research Development Program of China (Grant No. 2019YFB2203502), National Natural Science Foundation of China (Grant Nos. 11761161002, 61775243, and 61905291), Guangdong Basic and Applied Basic Research Foundation (Grant No. 2018B030308005), and Science and Technology Program of Guangzhou (Grant No. 201804020029).

References

[1] H. A. Macleod, "Thin-film optical filters," CRC Press, 2010.
[2] Z. Yu, H. He, X. Li, H. Qi, and W. Li, "Stress mechanism of pulsed laser-driven damage in thin film under nanosecond ultraviolet laser irradiation," *Chin Opt Lett.*, vol. 11, 2013, https://doi.org/10.3788/col201311.073101.
[3] Y. Wang, H. Zheng, Y. Sheng, et al., "Spatial filtering for high power laser beam by volume Bragg grating," In *2009 International Conference on Optical Instruments and Technology: Optical Systems and Modern Optoelectronic Instruments*, 2009.
[4] Y. Zhang, J. Zheng, Y. Wang, J. Zhao, and S. Ruan, "Design and fabrication of multilayer dielectric film for combination device spatial filter," *Optik*, p. 181, 2018, https://doi.org/10.1016/j.ijleo.2018.12.036.
[5] E. D. Kosten, J. H. Atwater, J. Parsons, A. Polman, and H. A. Atwater, "Highly efficient GaAs solar cells by limiting light emission angle," *Light-Sci Appl.*, vol. 2, e45, 2013, https://doi.org/10.1038/lsa.2013.1.
[6] E. D. Kosten, B. M. Kayes, and H. A. Atwater, "Experimental demonstration of enhanced photon recycling in angle-restricted GaAs solar cells," *Energy Environ Sci.*, vol. 7, pp. 1907–1912, 2014.
[7] Y. Young Keun and K. Joung Myoun, "Grating lobe suppression of phased array antenna for mobile satellite communications, 6th International SYmposium on Antennas," In *Propagation and EM Theory, 2003 Proceedings* 28 Oct.-1 Nov. 2003; 2003, pp 222–224, 2003.
[8] F. Scattone, M. Ettorre, R. Sauleau, N. T. Nguyen, and N. J. G. Fonseca, "Optimization procedure for planar leaky-wave antennas with flat-topped radiation patterns," *IEEE Trans Antennas Propag*, vol. 63, pp. 5854–5859, 2015.
[9] I. Moreno, J. J. Araiza, and M. Avendano-Alejo, "Thin-film spatial filters," *Opt Lett.*, vol. 30, pp. 914–916, 2005.
[10] S. Jiang, J. Li, J. Tang, and H. Wang, "Multi-channel and sharp angular spatial filters based on one-dimensional photonic crystals," *Chin Opt Lett.*, vol. 4, pp. 605–607, 2006.
[11] Y. Zhang, H. Qi, Yi, Y. Wang, Z. Sui, and J. Shao, "Analysis of the spatial filter of a dielectric multilayer film reflective cutoff filter-combination device," *Chin Phys B.*, vol. 24, pp. 104216, 2015.
[12] X. Jiang, C. Zhou, X. Yu, S. Fan, M. Soljačić, and J. D. Joannopoulos, "The nonlinear effect from the interplay between the nonlinearity and the supercollimation of photonic crystal," *Appl Phys Lett.*, vol. 91:031105, 2007, https://doi.org/10.1063/1.2739413.
[13] A. E. Serebryannikov, A. Y. Petrov, and E. Ozbay, "Toward photonic crystal based spatial filters with wide angle ranges of total transmission," *Appl Phys Lett.*, vol. 94, p. 181101, 2009.
[14] A. E. Serebryannikov, P. Lalanne, A. Y. Petrov, and E. Ozbay, "Wide-angle reflection-mode spatial filtering and splitting with photonic crystal gratings and single-layer rod gratings," *Opt Lett.*, vol. 39, pp.6193–6196, 2014.
[15] D. Peri and A. A. Friesem, "Image restoration using volume diffraction gratings," *Opt Lett.*, vol. 3, pp. 124–126, 1978.
[16] J. E. Ludman, J. R. Riccobono, N. O. Reingand, I. V. Semenova, Y. L. Korzinin, and M. S. Shahriar, "Holographic nonspatial filter," *SPIE*, vol. 2532, 1995.
[17] X. Zhang, X. Yuan, S. Wu, J. Feng, K. Zou, and G. Zhang, "Two-dimensional angular filtering by volume Bragg gratings in photothermorefractive glass," *Opt Lett.*, vol. 36, pp. 2167–2169, 2011.
[18] W. H. Southwell, "Spectral response calculations of rugate filters using coupled-wave theory," *J Opt Soc Am A.*, vol. 5, pp. 1558–1564, 1988.
[19] P. V. Usik, A. E. Serebryannikov, and E. Ozbay, "Spatial and spatial-frequency filtering using one-dimensional graded-index lattices with defects," *Opt Commun.*, vol. 282, pp. 4490–4496, 2009.
[20] Z. Luo, S. Wen, Z. Tang, H. Luo, Y. Xiang, and D. Song, "Low-pass rugate spatial filters for beam smoothing," *Opt Commun.*, vol. 283, pp. 2665–2668, 2010.

[21] G. Liang, P. Han, and H. Wang, "Narrow frequency and sharp angular defect mode in one-dimensional photonic crystals from a photonic heterostructure," *Opt Lett.*, vol. 29, pp. 192–194, 2004.
[22] S. Jiang, Y. Liu, G. Liang, and H. Wang, "Design and fabrication of narrow-frequency sharp angular filters," *Appl Optics.*, vol. 44, pp. 6353–6356, 2005.
[23] M. Shyiq Amin, J. Woong Yoon, and R. Magnusson, "Optical transmission filters with coexisting guided-mode resonance and Rayleigh anomaly," *Appl Phys Lett.*, vol. 103, p. 131106, 2013.
[24] C. F. R. Mateus, M. C. Y. Huang, Y. Deng, A. R. Neureuther, and C. J. Chang-Hasnain, "Ultrabroadband mirror using low-index cladded subwavelength grating," *IEEE Photon Technol Lett.*, vol. 16, pp. 518–520, 2004.
[25] Y. Kanamori, M. Shimono, and K. Hane, "Fabrication of transmission color filters using silicon subwavelength gratings on quartz substrates," *IEEE Photon Technol Lett.*, vol. 18, pp. 2126–2128, 2006.
[26] Y. Ding and R. Magnusson, "Resonant leaky-mode spectral-band engineering and device applications," *Opt Express.*, vol. 12, pp. 5661–5674, 2004.
[27] E. Sakr and P. Bermel, "Angle-selective reflective filters for exclusion of background thermal emission," *Phys Rev Appl.*, vol. 7, 2017, https://doi.org/10.1103/physrevapplied.7.044020.
[28] M. C. Y. Huang, Y. Zhou, and C. J. Chang-Hasnain, "A surface-emitting laser incorporating a high-index-contrast subwavelength grating," *Nat Photonics.*, vol. 1, pp. 119–122, 2007.
[29] F. Brückner, D. Friedrich, T. Clausnitzer, et al., "Realization of a monolithic high-reflectivity cavity mirror from a single silicon crystal," *Phys Rev Lett.*, vol. 104, 2010, https://doi.org/10.1103/physrevlett.104.163903.
[30] A. Arbabi, Y. Horie, M. Bagheri, and A. Faraon, "Dielectric metasurfaces for complete control of phase and polarization with subwavelength spatial resolution and high transmission," *Nat Nanotechnol.*, vol. 10, pp. 937–943, 2015.
[31] S. Liu, J. Zhuge, S. Ma, et al., "A bi-layered quad-band metamaterial absorber at terahertz frequencies," *J Appl Phys.*, vol. 118, pp. 245304, 2015.
[32] B. Yang, T. Liu, H. Guo, S. Xiao, and L. Zhou, "High-performance meta-devices based on multilayer meta-atoms: interplay between the number of layers and phase coverage," *Sci Bull.*, vol. 64, pp. 823–835, 2019.
[33] Y. Li, J. Lin, H. Guo, W. Sun, S. Xiao, and L. Zhou, "A tunable metasurface with switchable functionalities: from perfect transparency to perfect absorption," *Adv Opt Mater.*, vol. 8, p. 1901548, 2020.
[34] R. Magnusson and M. Shokooh-Saremi, "Physical basis for wideband resonant reflectors," *Opt Express.*, vol. 16, pp. 3456–3462, 2008.
[35] V. Karagodsky, F. G. Sedgwick, and C. J. Chang-Hasnain, "Theoretical analysis of subwavelength high contrast grating reflectors," *Opt Express.*, vol. 18, pp. 16973–16988, 2010.
[36] M. C. Y. Huang, Y. Zhou, and C. J. Chang-Hasnain, "A nanoelectromechanical tunable laser," *Nat Photonics.*, vol. 2, pp. 180–184, 2008.
[37] C. Chase, Y. Rao, W. Hofmann, and C. J. Chang-Hasnain, "1550 nm high contrast grating VCSEL," *Opt Express.*, vol. 18, pp. 15461–15466, 2010.
[38] T. Ansbaek, I. Chung, E. S. Semenova, and K. Yvind, "1060-nm tunable monolithic high index contrast subwavelength grating VCSEL," *IEEE Photon Technol Lett.*, vol. 25, pp. 365–367, 2013.
[39] K. Li, Y. Rao, C. Chase, W. Yang, and C. J. Chang-Hasnain, "Monolithic high-contrast metastructure for beam-shaping VCSELs," *Optica.*, vol. 5, pp. 10–13, 2018.
[40] B. W. Yoo, M. Megens, T. Chan, et al., "Optical phased array using high contrast gratings for two dimensional beamforming and beamsteering," *Opt Express.*, vol. 21, pp. 12238–12248, 2013.
[41] W. Yang, T. Sun, Y. Rao, et al., "High speed optical phased array using high contrast grating all-pass filters," *Opt Express.*, vol. 22, pp. 20038–20044, 2014.
[42] M. Niraula, J. W. Yoon, and R. Magnusson, "Single-layer optical bandpass filter technology," *Opt Lett.*, vol. 40, pp. 5062–5065, 2015.
[43] D. L. Brundrett, E. N. Glytsis, and T. K. Gaylord, "Normal-incidence guided-mode resonant grating filters: design and experimental demonstration," *Opt Lett.*, vol. 23, pp. 700–702, 1998.
[44] M. Niraula, J. W. Yoon, and R. Magnusson, "Concurrent spatial and spectral filtering by resonant nanogratings," *Opt Express.*, vol. 23, pp. 23428–23435, 2015.
[45] S. Boutami, B. Benbakir, X. Letartre, J. L. Leclercq, P. Regreny, and P. Viktorovitch, "Ultimate vertical Fabry-Perot cavity based on single-layer photonic crystal mirrors," *Opt Express.*, vol. 15, pp. 12443–12449, 2007.
[46] Y. Horie, A. Arbabi, S. Han, and A. Faraon, "High resolution on-chip optical filter array based on double subwavelength grating reflectors," *Opt Express.*, vol. 23, pp. 29848–298454, 2015.
[47] Y. Zhou, I. I. Kravchenko, H. Wang, H. Zheng, G. Gu, and J. Valentine, "Multifunctional metaoptics based on bilayer metasurfaces," *Light-Sci Appl.*, vol. 8, p. 80, 2019.
[48] Z. Wang, B. Zhang, and H. deng, "Dispersion engineering for vertical microcavities using subwavelength gratings," *Phys Rev Lett.*, vol. 114, 2015, https://doi.org/10.1103/physrevlett.114.073601.
[49] C. J Chang-Hasnain and W. Yang, "High-contrast gratings for integrated optoelectronics," *Adv Opt Photonics.*, vol. 4, pp. 379–440, 2012.
[50] V. Karagodsky, C. Chase, and C. J. Chang-Hasnain, "Matrix Fabry–Perot resonance mechanism in high-contrast gratings," *Opt Lett.*, vol. 36, pp. 1704–1706, 2011.
[51] J. Du, Z. Lin, S. Chui, G. Dong, and W. Zhang, "Nearly total omnidirectional reflection by a single layer of nanorods," *Phys Rev Lett.*, vol. 110, p. 163902, 2013.
[52] R. Hofmann, B. R. Brandl, A. Eckart, F. Eisenhauer, and L. E. Tacconi-Garman. *High-angular-resolution NIR astronomy with large arrays (SHARP I and SHARP II)*. SPIE. vol. 2475, 1995.
[53] T. Chen and C. Guestrin, "XGBoost: a scalable tree boosting system," In *Proceedings of the 22nd ACM SIGKDD International Conference on Knowledge Discovery and Data Mining*, Association for Computing Machinery: San Francisco, California, USA, pp. 785–794, 2016.
[54] H. Y Song, S. Kim, and R. Magnusson, "Tunable guided-mode resonances in coupled gratings," *Opt Express.*, vol. 17, pp. 23544–23555, 2009.